Since January 2020 Elsevier has created a COVID-19 resource centre with free information in English and Mandarin on the novel coronavirus COVID-19. The COVID-19 resource centre is hosted on Elsevier Connect, the company's public news and information website.

Elsevier hereby grants permission to make all its COVID-19-related research that is available on the COVID-19 resource centre - including this research content - immediately available in PubMed Central and other publicly funded repositories, such as the WHO COVID database with rights for unrestricted research re-use and analyses in any form or by any means with acknowledgement of the original source. These permissions are granted for free by Elsevier for as long as the COVID-19 resource centre remains active.

Applied Soft Computing Journal 103 (2021) 107160

Contents lists available at ScienceDirect

Applied Soft Computing Journal

journal homepage: www.elsevier.com/locate/asoc

DeepCoroNet: A deep LSTM approach for automated detection of COVID-19 cases from chest X-ray images

Fatih Demir

Firat University, Technology Faculty, Electrical-Electronics Engineering Department, Elazig, Turkey

ARTICLE INFO

Article history:
Received 2 October 2020
Received in revised form 9 January 2021
Accepted 28 January 2021
Available online 8 February 2021

Keywords:
COVID-19
Automated detection
Marker-controlled watershed segmentation
Deep LSTM model

ABSTRACT

The new coronavirus, known as COVID-19, first emerged in Wuhan, China, and since then has been transmitted to the whole world. Around 34 million people have been infected with COVID-19 virus so far, and nearly 1 million have died as a result of the virus. Resource shortages such as test kits and ventilator have arisen in many countries as the number of cases have increased beyond the control. Therefore, it has become very important to develop deep learning-based applications that automatically detect COVID-19 cases using chest X-ray images to assist specialists and radiologists in diagnosis. In this study, we propose a new approach based on deep LSTM model to automatically identify COVID-19 cases from X-ray images. Contrary to the transfer learning and deep feature extraction approaches, the deep LSTM model is an architecture, which is learned from scratch. Besides, the Sobel gradient and marker-controlled watershed segmentation operations are applied to raw images for increasing the performance of proposed model in the pre-processing stage. The experimental studies were performed on a combined public dataset constituted by gathering COVID-19, pneumonia and normal (healthy) chest X-ray images. The dataset was randomly separated into two sections as training and testing data. For training and testing, these separations were performed with the rates of 80%–20%, 70%–30% and 60%–40%, respectively. The best performance was achieved with 80% training and 20% testing rate. Moreover, the success rate was 100% for all performance criteria, which composed of accuracy, sensitivity, specificity and F-score. Consequently, the proposed model with pre-processing images ensured promising results on a small dataset compared to big data. Generally, the proposed model can significantly improve the present radiology based approaches and it can be very useful application for radiologists and specialists to help them in detection, quantity determination and tracing of COVID-19 cases throughout the pandemic.

© 2021 Elsevier B.V. All rights reserved.

1. Introduction

The new Coronavirus (COVID-19), which was first emerged in Wuhan, China in December 2019, is a member of virus family. Coronavirus was named firstly as SARS-CoV-2 by International Committee on Taxonomy of Viruses (ICTV) [1]. Then, its name was replaced with COVID-19 by World Health Organization (WHO) in February 2020. A Global Health Emergency reported that the COVID-19 disease broke out on 30 January 2020. Lastly, COVID-19 disease has been considered as a Pandemic since 11 March 2020 by WHO. With the outbreak, COVID-19 cases and deaths increased so quickly that the COVID-19 cases and deaths reached the numbers of 24,665,184 (active and recoveries) and 1,003,150, respectively, by 27 September 2020 [2]. The novel coronavirus with increasing death and case numbers has severely hit countries such as UK, USA, Italy, Spain, Brazil and India.

The COVID-19 disease may cause different symptoms and indications of infection which contain high fever, diarrhea, cough, respiratory diseases, and weakness. In some active cases, the COVID-19 may lead serious problems for the patient such as difficulty in breathing, pneumonia, multi-organ failure, sudden cardiac arrest, and death. The health care of many developed countries has come to a halt due to the exponential increase in active cases. Test kits and ventilators have become insufficient in countries with large numbers of active cases. The COVID-19 virus also paved the way for the increase in crisis. Therefore, many countries closed their borders with other countries. In addition, these countries banned domestic and international travels to their citizens and called for them to stay at home [3].

One of the most important steps to combat COVID-19 is to isolate infected patients from non-infected individuals as soon as possible. Real-time reverse transcription polymerase chain reaction (rRT-PCR) has been the most effective diagnosis method used to diagnose COVID-19 [4,5]. The test process is realized on respiratory patterns of the suspicious patient and the test

E-mail address: fatihdemir@firat.edu.tr.

https://doi.org/10.1016/j.asoc.2021.107160
1568-4946/© 2021 Elsevier B.V. All rights reserved.

outcomes can be obtained in few hours to 3 days. In addition, the methods based on chest radiological imaging such as computed tomography (CT) and chest X-ray (CX), can be considered as another diagnosis method [6,7]. With these methods, researchers have observed that the lungs of COVID-19 patients have some visual shapes such as marks and spots that can separate COVID-19 positive cases from COVID-19 negative cases [8]. Thus, these methods provide important clues for early diagnosis. Also, more precise results with these methods are achieved compared to the PTR screening method. Therefore, the researchers argue that radiological imaging based system may be a supplementary tool to conventional methods in detection, counting and pursuit of COVID-19 cases.

The radiological imaging based detection system has many superiorities over test kits based methods. It can give quick results and can be used for many patients at the same time. Therefore, it is very useful for hospitals in countries where test kits are not sufficient. Moreover, considering that there are radiological imaging systems in a hospital with average conditions, creating such a system will be both easy and cost-effective [9].

Nowadays, researchers working on different disciplines in many countries, deal with COVİD-19 virus intensely. To aid the decision making process of radiologists and specialists, some researchers have proposed papers explaining deep learning and machine learning based methods for automated COVID-19 detection from CT and CX images [10–12].

1.1. Related works

There are a number of machine learning based studies on respiratory diseases in the literature. In [13], Gray-level Co-occurrence Matrix (GLCM) was utilized to extract hand-crafted features from CT images. To measure the performances of hand-crafted features, the proposed method was evaluated with six-classifier. The highest accuracy was achieved as 0.89 with Random Forest Classifier. In [14], the local features were extracted from CX images by using descriptors containing grayscale histogram, GLCM texture-based features, and local binary pattern (LBP) algorithms. This model, which the features were reduced with a multi-objective genetic algorithm, was classified with a neuro-fuzzy classifier. In [12], the feature set used for automated COVID-19 detection using CX images was constituted with Residual Exemplar LBP algorithm. The hand-crafted features reduced with Relief algorithm were classified by SVM classifier. The best accuracy was 100% for 2-class (normal and COVID-19) classification problem. In sum, high performances can be achieved with the machine learning based approaches for automated COVID-19 detection. However, it may be necessary to re-adjust or change the descriptive algorithms used as evaluation conditions and datasets change. In this case, it requires additional computational cost and time. In addition, deep learning-based approaches are more appropriate to changing conditions than machine learning-based approaches that include hand-crafted features since deep learning approaches do not need hand-crafted features due to extracting the features from particular part of dataset in deep learning models. Moreover, the weight parameters of the pre-trained deep models such as VGGNet, AlexNet, and ResNet are publicly available for evaluating with different classification and regression problems. Therefore, many researchers have conducted studies involving deep learning models for automatic diagnosis of COVID-19 disease.

Hemdan et al. [15] utilized a deep learning approach to detect COVID-19 from CX data and constituted the COVIDX-Net structure including six CNN structure. Wang and Wong [11] constituted a deep learning model for COVID-19 automatic diagnosis. This model achieved 92.4% classification accuracy in detection of 3 classes with normal, pneumonia, and COVID-19 labels. Ioannis et al. [16] improved a deep learning structure, which used 224 approved CT images as input. These structure reached to 98.75% and 93.48% accuracy scores for 2 and 3 classes, respectively. Narin et al. [10] used the ResNet50 model to identify COVID-19 from CX images. Their method achieved a 98% classification accuracy. The best classification score with this structure involving the ResNet50 model was obtained as 95.38%. Y. Pathak et al. [17], used CT images and the transfer learning technique, which was utilized in CNN models to automatically diagnose COVID-19, and achieved a high classification performance. Togacar et al. [18] proposed an automatic detection algorithm using CX images for COVID-19 disease. In this study, CNN models such as AlexNet, VGG-16, and VGG-19 were used for deep feature extraction. With SVM classifier, the best accuracy score for the used dataset was concluded as 99.41%. Ismael et al. [19] used a comprehensive approach for COVID-19 detection based on CX images. Researchers used three deep CNN learning approaches for efficient COVID-19 detection. In addition, they used some local texture descriptors and SVM for COVID-19 detection. Ali Abbasian Ardakani et al. [20] utilized the popular deep learning models such as VGGNet, SqueezeNet, Xception, ResNet to detect COVID-19 disease and evaluated them with each other according to the accuracy criteria. Ferhat Ucar et al. [21] presented a new approach named Deep Bayes-SqueezeNet to perform binary classification (COVID-19 and normal) from X-ray images. Tulin Ozturk et al. [22] proposed a new approach based on deep learning called the DarkCovid-Net model, which had 17 convolutional layers and applied various filters on each layer, for the detection of COVID-19 disease. Ismael et al. [23] also used multiresolution approaches namely, Shearlets, Wavelets, and Contourlet transforms for COVID-19 detection. The researchers represented more improved results than the deep learning method's achievements.

1.2. Research problem statement and contributions

In this study, a novel approach was proposed for automated COVID-19 detection. A deep LSTM architecture named the DeepCoronet was used for training from processed CX images. Contributions of proposed method can be explained as follows:

- The performance of the DeepCoroNet was boosted with processed images constituted with MCWS algorithm.
- Classical LSTM models were inclined to overfitting, it was hard to implement the dropout layer to prevent this problem. Therefore, the dropout layer was used in the DeepCoroNet model.
- In the DeepCoroNet, the convolutional layer was used before the LSTM layer to make the characteristic details of the CX images more apparent.
- DeepCoroNet model after trained with big datasets, could be used in real-world applications for helping radiologists and specialists.

Limitations of proposed method can be explained as follows:

- The MCWS algorithm increases computational time of the proposed method.
- Deep LSTM based approach requires high memory bandwidth for real-world applications.

2. Dataset

A total of 1061 CX images obtained from different open public data was included in the dataset. The labeling processes were taken place by radiologists and specialists. CX images were rearranged under folders as COVID-19, Normal, and Pneumonia.

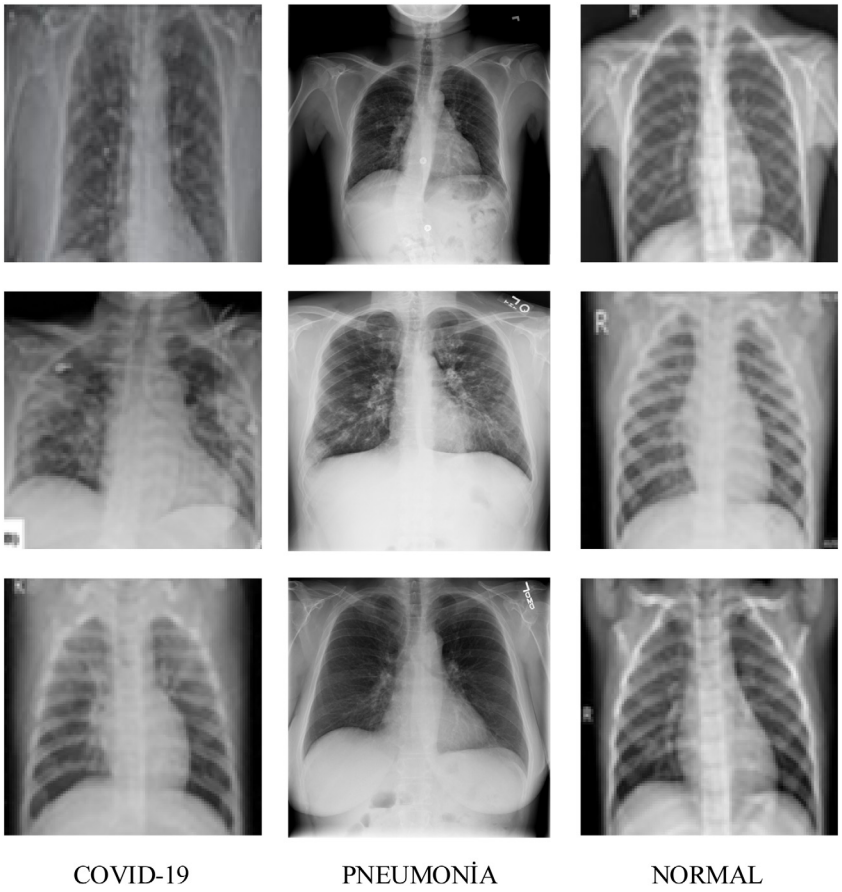

Fig. 1. CX image samples in the dataset.

COVID-19, Normal, and Pneumonia folders had 361, 200 and 500 CX images, respectively. 200 of the COVID-19 cases were male while 161 of them were female, and all cases were generally over 45 years old. The COVID-19 and normal (healthy) CX images were downloaded and arranged from Kaggle web sites [24,25]. The samples of pneumonia class were added from the dataset constituted by Wang et al. [15]. CX image samples for each class are shown in Fig. 1. As shown Fig. 1, CX image samples taking part in first, second and third column belong to the COVID-19, pneumonia and normal classes, respectively.

3. Techniques and method

3.1. Methodology

In this paper, a new and effective method was proposed to detect COVID-19 virus with high accuracy. The proposed method, presented in Fig. 2, was evaluated on the dataset composing of CX images. The proposed method was constituted with two stages, which contains the pre-processing and the deep LSTM model. In the first stage, the pre-processing techniques were applied to the CX images for increasing the classification performance. The first step of pre-processing was gradient operation by using Sobel operator. The gradient operator was used for emphasizing the spot regions in the CX images. In other words, gradient operator was used for improving the performance of the marker-controlled watershed segmentation (MCWS). In the second step, the MCWS was used to segment the spots on the gradient images. Actually, segmentation was used to reduce the number of the gray tones of the input CX images. In the last step, these processed images were resized for fitting the input layer of the deep LSTM model, which consisted of the sequence data creating block and the LSTM network. For the evaluation of the proposed method in the last stage, the deep LSTM model was created by using CNN based layers and LSTM layer. In the sequence data creating block, the resized MCWS images were converted to the sequence data (1D-vector) for the LSTM network input. In this block, convolutional operations were used for both input size decrease and pre-feature extraction. In the deep LSTM model, the LSTM network block was utilized for training and testing operations. The proposed LSTM network composed of 5 layers, which included the LSTM, the fully connected, the Rectified Linear Unit (ReLU), the dropout, and the softmax layers. The classification process was performed with the activation function in the softmax-layer.

3.2. Preprocessing

For input images in the gradient method, gradient magnitudes and directions are computed using directional gradient. These gradient operations are carried out with a gradient operator such as Sobel, Roberts and Prewitt [26].

In the watershed transformation, surfaces including light pixel density are high. In other words, surfaces including dark pixel density are low. Thus, catchment basins and watershed ridge lines in an image, are found with the watershed transformation [27]. In the watershed transformation, considering function $g \in C(S)$ have minimum $\{m_k\}_{k\in F}$ for a set F, the catchment basin $CB(m_j)$ of a minima m_j is described as the set of points (x) which are topographically closer to m_j than to another local minima m_i:

$$CB\left(m_j\right) = \left\{x \in S \mid \nabla i \in F\{i\} : \; g(m_j) + T_f\left(x, m_j\right) < g(m_i) + T_f\left(x, m_i\right)\right\} \quad (1)$$

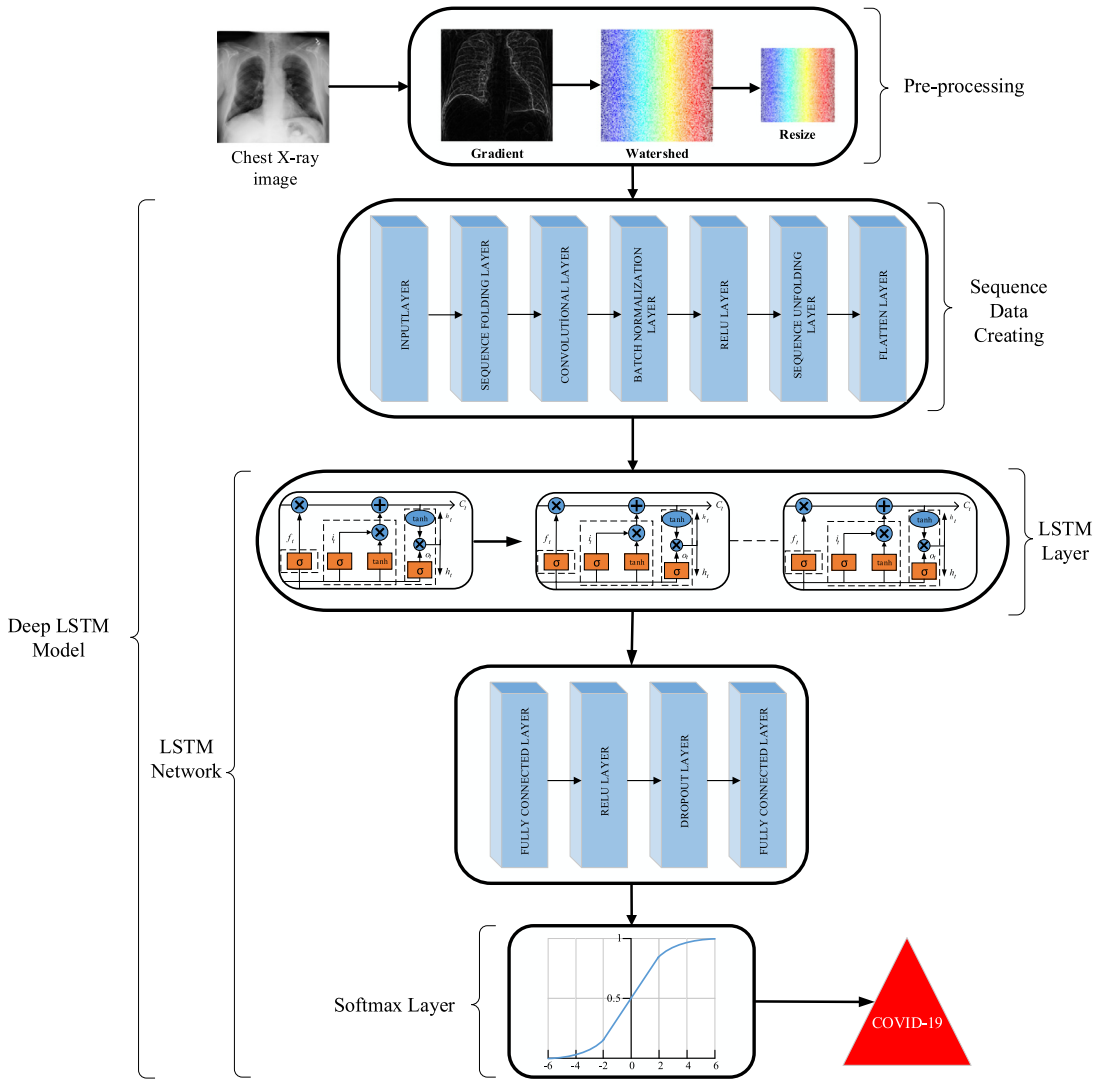

Fig. 2. Representation of the proposed method.

where S and T_f are domain and topographical distance, respectively. The watershed transformation of g ($Wshed(g)$) is the set of points that do not relate to any CB:

$$Wshed\,(g) = S \cap \left(\cup_{j\in F} CB\left(m_j\right)\right) \tag{2}$$

Considering $Wshed$ be a tag, $Wshed \notin F$, and $Wshed\,(g)$ is a mapping $\beta : S \to F \cup Wshed$.

The MCWS has been expressed to be a robust and valid algorithm to separate objects with covered shapes, where the borders are stated as ledges. Markers are inserted into the related objects. The inner and exterior markers are assigned to the related objects and backgrounds, respectively. At the end of segmentation, the borders of the watershed areas are constituted on the targeted ledges by dividing each object from its neighbors. Thus, the MCWS algorithm can separate each small or large detail that stands out in a radiological image regionally. MCWS algorithm composes of these basic steps:

- Calculate a segmentation operation used to separate dark regions into objects.
- Calculate foreground markers, which have the connected pixel blots inside each of the objects.
- Calculate background markers, which denote pixels not belonging to any object.
- Re-arrange for minimizing the function of segmentation at the foreground and background marker locations.
- Calculate the watershed transform with the updated parameters.

3.3. Deep learning techniques

In the sequence folding layer, a group of image sequences is converted to a group of images and convolution operations are applied to these image sequences by using time steps. In the sequence unfolding layer, the data coming from the sequence folding layer is transformed to sequence structure.

Convolution layer for a CNN is the main structure layer which utilizes convolution operation symbolized as "$*$", instead of general matrix multiplication [28–30]. Learnable parameters in this layer occur a set of learnable filters also called as kernels. The core function of the convolutional layer is to extract features taking part within local regions of the input data, which are similar along the dataset, and assigning their view to a feature map. The 2D convolution operation for discrete-time signals is given as Eq. (3).

$$(X * K)\,(i,j) = \sum_m \sum_n K\,(m,n)\,X(i-m, j-n) \tag{3}$$

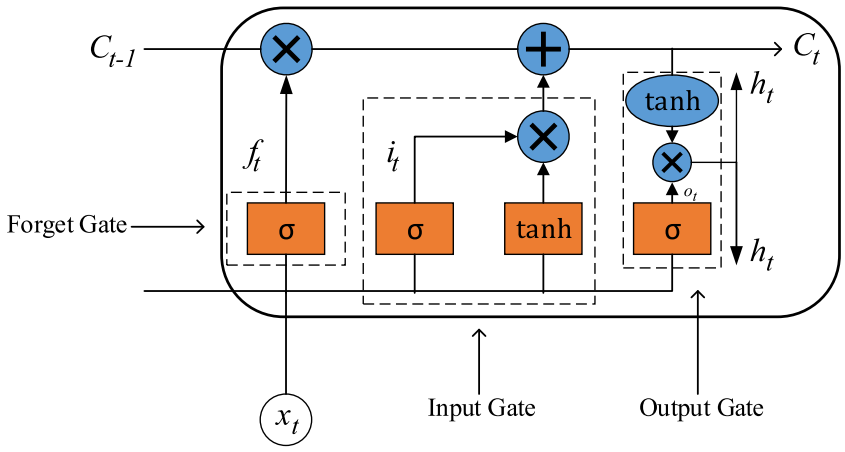

Fig. 3. Structure of the LSTM cell.

where X and K represent the input signal and 2D filter (kernel), respectively.

Batch normalization (BN) layer is used for two main purposes. One is to reduce training time of deep learning models, the other is to improve network initialization performance. Also, this layer is preferred to minimize the gradient vanishing problem. Variables used in the BN layer are calculated as given in Eqs. (4)–(7):

$$m_b = \frac{1}{n}\sum_{i=1}^{n} x_i \tag{4}$$

$$v_b = \frac{1}{n}\sum_{i=1}^{n} (x_i - m_b)^2 \tag{5}$$

$$\hat{x}_i = \frac{x_i - m_b}{\sqrt{v_b^2 + \varepsilon}} \tag{6}$$

$$y_i = a\hat{x}_i + b \tag{7}$$

where m_b and v_b are mini batch mean and mini batch variance, respectively. The normalized activation $\hat{x}_i$ is computed as shown in Eq. (6). Constant ε is added to improve the numerical operation, in case v_b is very small. Balance factor a and scale factor b are learnable parameters, and they are continuously updated to find the most convenient BN layer output (y_i) during optimization process [31–33].

In deep learning models, the convolution layer output conveys to a nonlinearity layer. The nonlinearity layer named also the activation layer gives to the training operation a nonlinearity characteristic [34]. To decrease the gradient vanishing and gradient explosion problem in deep learning models, the activation function, which is preferred in place of the sigmoid and tangent function used commonly for artificial neural networks (ANN), is ReLU function. In the ReLU layer, if the input is negative, it becomes equal to zero, otherwise the input is equal to output. It can be defined as follows.

$$f(x) = \max(0, x) \tag{8}$$

The flatten layer converts 2D data structure transmitted from convolution and ReLU layers to 1D data structure.

LSTM model is a modified version of recurrent neural network (RNN). The general LSTM cell has a control system, which consist of input, output and forget gates. The architecture of a LSTM cell is shown in Fig. 3. The LSTM cell memorizes values until a defined previous time interval, and three gates control the data traffic in input and output of the cell [35]. Also, the LSTM layer efficiently prevents the problem of gradient vanishing and explosion.

The operation mechanism of forget gate looks like a single layer neural network. The activation state of the forget gate is computed as shown in Eq. (9).

$$f_t = \sigma(W[x_t, h_{t-1}, C_{t-1}] + b_f) \tag{9}$$

where, x_t is input vector to the LSTM cell, h_{t-1} is output of previous LSTM cell, C_{t-1} is memory of previous LSTM cell, b_f is biased vector, W is weight vector, and σ is logistic sigmoid function. The input gate is a part which the current memory is constituted by a simple neural network with the hyperbolic tangent function and the previous memory cell activation values. These calculations are given in Eqs. (10) and (11).

$$i_t = \sigma(W[x_t, h_{t-1}, C_{t-1}] + b_i) \tag{10}$$

$$C_t = f_t.C_{t-1} + i_t.\tanh([x_t, h_{t-1}, C_{t-1}]) + b_c \tag{11}$$

The data and information coming from blocks of current LSTM cell are conveyed to the output gate. The output calculations are shown in Eqs. (12) and (13).

$$\sigma_t = \sigma(W[x_t, h_{t-1}, C_{t-1}] + b_o) \tag{12}$$

$$h_t = o_t.\tanh(C_t) \tag{13}$$

The fully connected layer connects all neurons of the previous and next layers to each other. The values of neurons give information about the extent to which a value matches the particular class [36]. The values in last fully connected layer is conveyed to the softmax layer, which gives the probable scores of classes. The dropout layer, which aids obstruct overfitting, randomly equalizes some input values to zero with a certain possibility during training process [37]. The softmax layer is utilized as the main classifier in CNN. The softmax activation function is given in Eq. (14).

$$S^k = \frac{e^{x^k}}{\sum_{i=1}^{n} e^{x^n}} \tag{14}$$

where x and S are the input vector and the output vector, respectively. In this function, all output sums (S) equals to one [38].

3.4. Method evaluation

The confusion matrix showing the true positive (TP), true negative (TN), false positive (FP), false negative (FN) numbers was used to evaluate the performance of proposed method. The accuracy (Acc), sensitivity (Sn), specificity (Sp), precision (Pr) and F-score values were utilized as the performance metrics. These metrics were computed as the following equations.

$$Acc = \frac{TP + TN}{TP + TN + FP + FN} \tag{15}$$

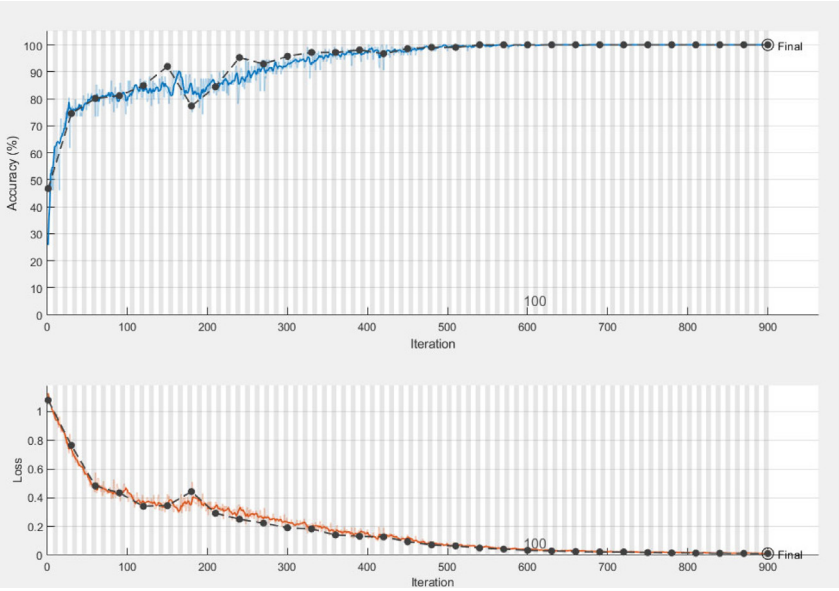

Fig. 4. The graphs of accuracy and loss values for the training and validation.

$$Sn = \frac{TP}{TP + FN} \tag{16}$$

$$Sp = \frac{TN}{TN + FP} \tag{17}$$

$$Pr = \frac{TP}{TP + FP} \tag{18}$$

$$F - score = \frac{2 \times TP}{2 \times TP + FP + FN} \tag{19}$$

4. Experimental setup and results

The experimental works were performed on a work station with Intel® Core™ i7-5500U, 2 GB graphics card, 8 GB memory card. The simulation operation was carried out with the MATLAB(2020a) programming language.

The height and width of MCWS images were resized to 100 ×100 for the input layer. The filter size and numbers in the convolutional layer were set to 5 and 20, respectively. To not increase the elapsed time of the training, the hidden layer number of the LSTM layer was adjusted to 100.

To evaluate the proposed method, the dataset was randomly divided as the training data and testing data. The training and testing data were evaluated in the proposed model at 0.8–0.2 (training–testing), 0.7–0.3 (training–testing) and 0.6–0.4 (training–testing) ratios, respectively. The max epoch, iteration and iterations per epoch values which were the fixed training parameters, were set as 150, 900 and 6, respectively. The validation results were adjusted to give results in every 30 iterations. The initial learning rate was selected as 0.001. The learning drop factor and the learning drop period was adjusted to 0.1 and 10, respectively, for the learning rate that gradually decreased during the training process. The stochastic gradient descent with momentum (SGDM) algorithm was chosen for the optimization operation of learnable parameters. The elapsed time of the training and testing was 53 min and 22 s For training data with 80 percent of the entire dataset, the graphs of training–testing(validation) accuracies and training–testing loss values were given in Fig. 4.

At the end of 900 iterations, as seen in Fig. 4, training and testing accuracies reached to 100% when training and testing loss values reduced to 0, and the computation time for training process of DeepCoroNet was 53 min 22 s.

As a result of the activation with the layer operations of the inputs along the deep learning models, the important alterations can occur in the activation maps, and the situation of the layers in the training stage can be monitored using activation outputs. The main target in the deep learning layers is to extract the activations that have the most discriminative characteristics compared to others involving less representation ability. Many filter and activation operations are utilized in the deep learning approaches, and the inputs are processed in these operations. The attributes involving the main shapes and colors are learned through the first filter operations of deep learning models, while attributes that need more detail are learned in later filter operations. Also, finding the activations giving the best performance is a very difficult process since the performance of activations can change depending on the types of the challenges. The visual representation of the optimized activation outputs of the convolutional, LSTM and last fully connected layers for all classes is shown in Fig. 5. As can be seen from Fig. 5, activation dimensions are reduced until they reach the last fully connected layer. The activation output visual of the last fully connected layer in the first, second and third rows in Fig. 5 gives information about the input samples belong to the COVID-19, normal and pneumonia classes, respectively.

For raw images, MCWS images (rows) and the rates of training–testing (columns), the confusion matrix results are given in Fig. 6. According to these confusion matrix results, other performance criteria results, which consist of sensitivity, specificity, precision and F-score, are shown in Table 1. As can be seen from Fig. 6 and Table 1, the evaluations with MCWS images gave better results than the evaluations with raw images. In the evaluations performed with MCWS images, the best performance scores were achieved with 80% training and 20% test rates. Besides, the deep LSTM model using the MCWS images as input outperformed the same model using the raw images as input. For example, accuracy results in the evaluation, which was performed with MCWS images for 80%–20%, 70%–30%, and 60%–40% training–testing rates, increased by 2.64%, 1.57% and 3.77%, respectively. In Table 1, the worst result in the evaluation made for all classes was achieved as 0.81 for the precision criterion of the normal class, which was obtained from 60%–40% training–testing rate and raw images.

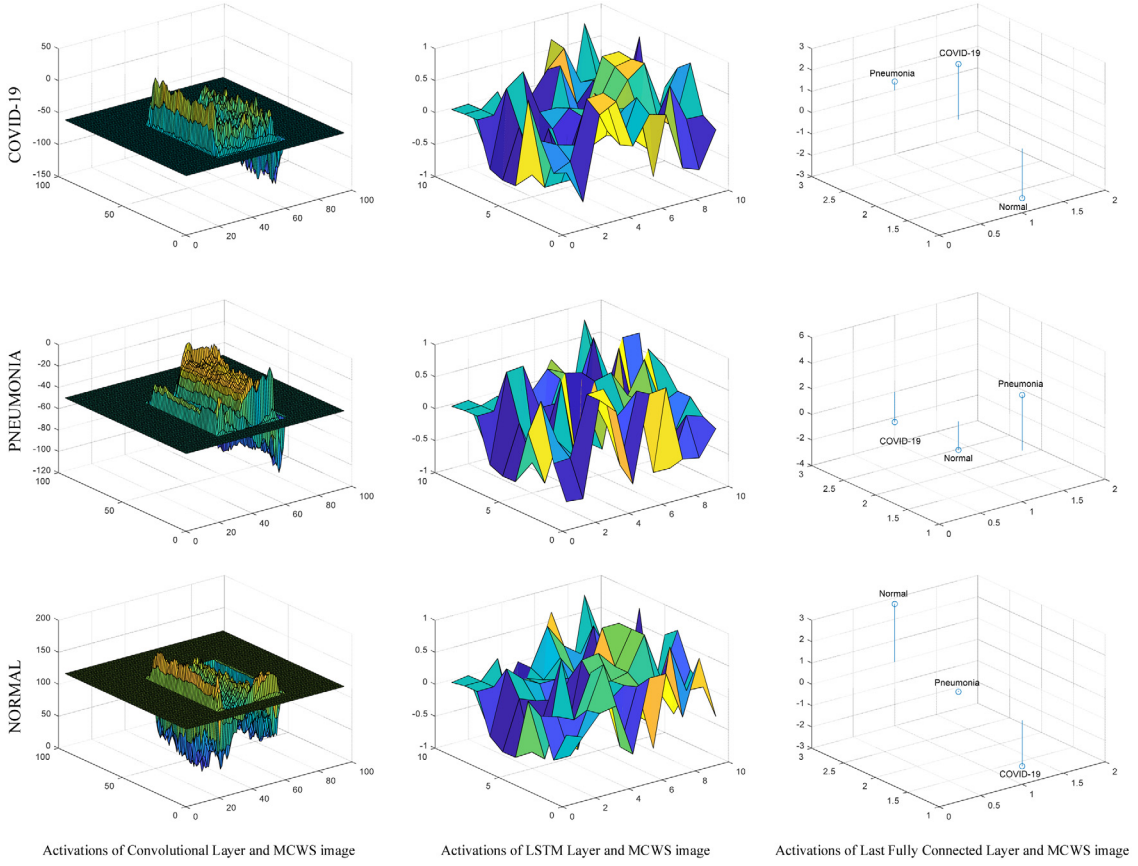

Fig. 5. Optimized activation outputs of deep LSTM network.

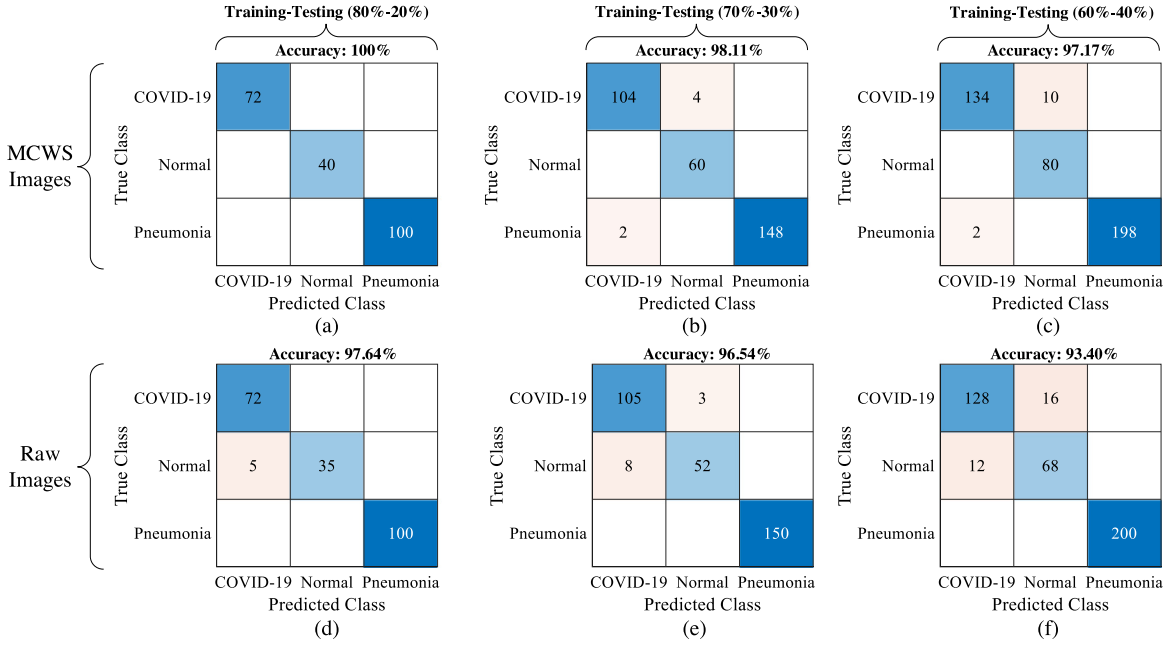

Fig. 6. Confusion matrix results for input images, MCWS images and the rates of training–testing..

5. Discussion

In this section, the state-of-the-art methods and the proposed method are discussed according to performance criteria, which consist of accuracy, sensitivity and specificity. However, it cannot be said that the methods are completely superior to each other due to the different datasets and evaluation criteria. In addition, big datasets, which give more valid and better results in deep learning, are completely not organized because the COVID-19 virus has just emerged. For this reason, the evaluations in the literature is generally performed on the combined datasets. The performance scores of these methods are given in Table 2.

Table 1
Performance criteria for training–testing rate and types of images.

training–testing rates (%)	Type of images	Classes	Sn	SP	Pr	F-score
80–20	MCWS	COVID-19	1,00	1,00	1,00	1,00
		Normal	1,00	1,00	1,00	1,00
		Pneumonia	1,00	1,00	1,00	1,00
70–30	MCWS	COVID-19	0,96	0,99	0,98	0,97
		Normal	1,00	0,98	0,94	0,97
		Pneumonia	0,99	1,00	1,00	0,99
60–40	MCWS	COVID-19	0,93	0,99	0,99	0,96
		Normal	1,00	0,97	0,89	0,94
		Pneumonia	0,99	1,00	1,00	1,00
80–20	Raw	COVID-19	1,00	0,96	0,94	0,97
		Normal	0,88	1,00	1,00	0,93
		Pneumonia	1,00	1,00	1,00	1,00
70–30	Raw	COVID-19	0,97	0,96	0,93	0,95
		Normal	0,87	0,99	0,95	0,90
		Pneumonia	1,00	1,00	1,00	1,00
60–40	Raw	COVID-19	0,89	0,96	0,91	0,90
		Normal	0,85	0,95	0,81	0,83
		Pneumonia	1,00	1,00	1,00	1,00

Table 2
The performance scores of the state-of-the-art methods and the proposed method.

Methods	Dataset	Number of classes	Acc (%)	Se (%)	Sp (%)
DarkCovidNet [22]	Public	3	87.02	92.18	89.96
COVIDiagnosis-Net [21]	Public	3	98.26	99.13	–
The pretrained CNNs [16]	Public	3	93.48	92.85	98.75
COVID-Net [11]	Public	3	92.64	91.37	95.76
Deep features, ResNet-50, SVM [39]	Public	2	95.38	–	–
Deep CNNs [40]	Public	2	90.00	100.00	80.00
Deep CNN, ResNet-50 [10]	Public	2	98.00	–	–
DRE-Net, deep CNN [41]	Private	2	86.00	96.00	–
Deep CNN, Inception, transfer learning [42]	Private	2	89.50	87.00	88.00
nCOVnet, transfer learning, deep CNN [43]	Public	2	88.10	97.62	89.13
Deep CNN, SVM [44]	Public	3	98.97	89.39	99.75
Proposed Method	Public	3	100	100	100

Ozturk et al. [22] proposed a deep learning architecture composing of 17 convolutional layers for automatic detection of COVID-19 virus on a data set with 3 classes. The best accuracy score was 87.02% with the 5-fold cross validation. Ucar et al. [21] learned the best hyperparameters of the pre-trained the SequeezeNet model with Bayes Optimization algorithm for the 3-class COVID-19 problem. Their model achieved a 98.26% accuracy score using the data augmentation. Apostolopoulos et al. [16] opted for the transfer learning method using VGG19, MobileNet v2, Inception, Xception and Inception ResNet v2 models to categorize the COVID-19 virus. The best accuracy was 93.48% with this method. Wang et al. [11] reached an accuracy of 92.64% with an end-to-end deep learning model involving many convolutional layers for COVID-19 classification problem. For feature extraction and classification, Sethy et al. [39] constituted a hybrid method using deep learning models and SVM algorithm, respectively. The best accuracy was 95.38% for binary classification. Similar to [10,40–44], the transfer learning, deep feature extraction and end-to-end deep learning algorithms were used to detect the COVID-19 virus automatically from CX images.

The current study presents a novel deep LSTM model that is learned from scratch instead of transfer learning or deep feature extraction approach. MCWS images were created instead of using a raw image and the algorithm were conveyed to deep LSTM model in the pre-processing stage. MCWS images increased performance of deep LSTM based model. However, computation cost is required for creating MCWS images. The proposed model was trained and tested for different ratios of all dataset. Best scores were obtained at a training-test ratio of 80%–20%. This shows that as the training data increased, the performance of the proposed method increased. Therefore, as the number of COVID-19 cases increases, retraining the proposed model can increase its success rate. However, the performance of the proposed model will decrease if the CX images added to the training set is low resolution and noisy.

The proposed approach reached to 100% success rate in accuracy, sensitivity and specificity criteria. It could not be argued that the proposed method is completely superior to other methods in the literature because of the fact that an organized dataset that everyone can use has not yet been created for COVID-19 disease. In the future, the performance of the proposed method can be tested more reliably with a challenge dataset. In addition, the proposed model can be adapted to automatically detect all respiratory diseases in addition to COVID-19 and pneumonia. In addition, this model, which is associated with a GUI interface, can be used as a supportive tool in the decision-making process of experts, radiologists and physicians.

6. Conclusion

As COVID-19 cases are increasing every day, the increasing number of deaths and economic crises in many countries with resource shortages continue to affect social life adversely. During the pandemic period, as studies on the COVID-19 virus go on, the virus transmission from COVID-19 patients, which cannot be diagnosed correctly, to the healthy people will increase the size of the pandemic. Therefore, a new approach that detects COVID-19 disease with high accuracy from CX images was proposed in the present study. The proposed method based on the deep LSTM model gave a high success rate for three-classes classification problem that composed of COVID-19, pneumonia and normal. It was also observed that using the MCWS images instead of the

raw image as input in the deep LSTM model increased the classification performance. With the 80%–20% training–testing rate, the best performance was achieved as 100% in all criteria involving accuracy, sensitivity, precision and F-score. In this period, artificial intelligence-based applications with high success rates will provide great support to experts in the decision-making process, since the Covid-19 cases increase excessively. A single expert can detect more COVID-19 cases in one day since the increase in the number of cases can be prevented with this method, which has a high success with a small number of samples.

Declaration of competing interest

The authors declare that they have no known competing financial interests or personal relationships that could have appeared to influence the work reported in this paper.

References

[1] F. Wu, S. Zhao, B. Yu, Y.-M. Chen, W. Wang, Z.-G. Song, Y. Hu, Z.-W. Tao, J.-H. Tian, Y.-Y. Pei, et al., A new coronavirus associated with human respiratory disease in China, Nature 579 (2020) 265–269.

[2] E. Mahase, Coronavirus: covid-19 has killed more people than SARS and MERS combined, despite lower case fatality rate, 2020.

[3] N. Chen, M. Zhou, X. Dong, J. Qu, F. Gong, Y. Han, Y. Qiu, J. Wang, Y. Liu, Y. Wei, et al., Epidemiological and clinical characteristics of 99 cases of 2019 novel coronavirus pneumonia in Wuhan, China: a descriptive study, Lancet 395 (2019) 507–513.

[4] W. Wang, Y. Xu, R. Gao, R. Lu, K. Han, G. Wu, W. Tan, Detection of SARS-CoV-2 in different types of clinical specimens, JAMA - J. Am. Med. Assoc. 323 (2020) 1843–1844, http://dx.doi.org/10.1001/jama.2020.3786.

[5] V.M. Corman, O. Landt, M. Kaiser, R. Molenkamp, A. Meijer, D.K.W. Chu, T. Bleicker, S. Brünink, J. Schneider, M.L. Schmidt, D.G.J.C. Mulders, B.L. Haagmans, B. Van Der Veer, S. Van Den Brink, L. Wijsman, G. Goderski, J.L. Romette, J. Ellis, M. Zambon, M. Peiris, H. Goossens, C. Reusken, M.P.G. Koopmans, C. Drosten, Detection of 2019 novel coronavirus (2019-nCoV) by real-time RT-PCR, Eurosurveillance 25 (2020) 2000045, http://dx.doi.org/10.2807/1560-7917.ES.2020.25.3.2000045.

[6] A. Bernheim, X. Mei, M. Huang, Y. Yang, Z.A. Fayad, N. Zhang, K. Diao, B. Lin, X. Zhu, K. Li, S. Li, H. Shan, A. Jacobi, M. Chung, Chest CT findings in coronavirus disease 2019 (COVID-19): Relationship to duration of infection, Radiology 295 (2020) 685–691, http://dx.doi.org/10.1148/radiol.2020200463.

[7] Y. Fang, H. Zhang, J. Xie, M. Lin, L. Ying, P. Pang, W. Ji, Sensitivity of chest CT for COVID-19: Comparison to RT-PCR, Radiology. 296 (2020) E115–E117, http://dx.doi.org/10.1148/radiol.2020200432.

[8] X. Xie, Z. Zhong, W. Zhao, C. Zheng, F. Wang, J. Liu, Chest CT for typical coronavirus disease 2019 (COVID-19) pneumonia: Relationship to negative RT-PCR testing, Radiology 296 (2020) E41–E45, http://dx.doi.org/10.1148/radiol.2020200343.

[9] S. Jin, B. Wang, H. Xu, C. Luo, L. Wei, W. Zhao, X. Hou, W. Ma, Z. Xu, Z. Zheng, et al., AI-Assisted CT imaging analysis for COVID-19 screening: Building and deploying a medical AI system in four weeks, 2020, MedRxiv.

[10] A. Narin, C. Kaya, Z. Pamuk, Automatic detection of coronavirus disease (COVID-19) using X-ray images and deep convolutional neural networks, 2020, http://arxiv.org/abs/2003.10849, ArXiv Prepr, arXiv:2003.10849.

[11] L. Wang, Z.Q. Lin, A. Wong, COVID-Net: a tailored deep convolutional neural network design for detection of COVID-19 cases from chest X-ray images, Sci. Rep. 10 (2020) http://dx.doi.org/10.1038/s41598-020-76550-z.

[12] T. Tuncer, S. Dogan, F. Ozyurt, An automated Residual Exemplar Local Binary Pattern and iterative Relief based corona detection method using lung X-ray image, Chemom. Intell. Lab. Syst. 203 (2020) 104054, http://dx.doi.org/10.1016/j.chemolab.2020.104054.

[13] J.T.C. Ming, N.M. Noor, O.M. Rijal, R.M. Kassim, A. Yunus, Lung disease classification using reticular pattern scoring and five class features with greedy stepwise based on GLCM, in: IEEE Reg. 10 Annu. Int. Conf. Proceedings/TENCON, 2017, pp. 182–186, http://dx.doi.org/10.1109/TENCON.2017.8227858.

[14] S. Varela-Santos, P. Melin, A new modular neural network approach with fuzzy response integration for lung disease classification based on multiple objective feature optimization in chest X-ray images, Expert Syst. Appl. 168 (2020) 114361, http://dx.doi.org/10.1016/j.eswa.2020.114361.

[15] X. Wang, Y. Peng, L. Lu, Z. Lu, M. Bagheri, R.M. Summers, ChestX-ray: Hospital-scale chest X-ray database and benchmarks on weakly supervised classification and localization of common thorax diseases, in: Adv. Comput. Vis. Pattern Recognit., 2019, pp. 369–392, http://dx.doi.org/10.1007/978-3-030-13969-8_18.

[16] I.D. Apostolopoulos, T.A. Mpesiana, Covid-19: automatic detection from X-ray images utilizing transfer learning with convolutional neural networks, Phys. Eng. Sci. Med. 43 (2020) 635–640, http://dx.doi.org/10.1007/s13246-020-00865-4.

[17] Y. Pathak, P.K. Shukla, A. Tiwari, S. Stalin, S. Singh, Deep transfer learning based classification model for COVID-19 disease, Irbm. (2020) http://dx.doi.org/10.1016/j.irbm.2020.05.003.

[18] M. Toğaçar, B. Ergen, Z. Cömert, COVID-19 detection using deep learning models to exploit social mimic optimization and structured chest X-ray images using fuzzy color and stacking approaches, Comput. Biol. Med. 121 (2020) 103805, http://dx.doi.org/10.1016/j.compbiomed.2020.103805.

[19] A.M. Ismael, A. Şengür, Deep learning approaches for COVID-19 detection based on chest X-ray images, Expert Syst. Appl. 164 (2021) 114054, http://dx.doi.org/10.1016/j.eswa.2020.114054.

[20] A.A. Ardakani, A.R. Kanafi, U.R. Acharya, N. Khadem, A. Mohammadi, Application of deep learning technique to manage COVID-19 in routine clinical practice using CT images: Results of 10 convolutional neural networks, Comput. Biol. Med. 121 (2020) 103795, http://dx.doi.org/10.1016/j.compbiomed.2020.103795.

[21] F. Ucar, D. Korkmaz, COVIdiagnosis-net: Deep Bayes-squeezenet based diagnostic of the coronavirus disease 2019 (COVID-19) from X-ray images, Med. Hypotheses. 140 (2019) 109761.

[22] T. Ozturk, M. Talo, E.A. Yildirim, U.B. Baloglu, O. Yildirim, U. Rajendra Acharya, Automated detection of COVID-19 cases using deep neural networks with X-ray images, Comput. Biol. Med. 121 (2020) 103792, http://dx.doi.org/10.1016/j.compbiomed.2020.103792.

[23] A.M. Ismael, A. Şengür, The investigation of multiresolution approaches for chest X-ray image based COVID-19 detection, Heal. Inf. Sci. Syst. 8 (2020) 1–11, http://dx.doi.org/10.1007/s13755-020-00116-6.

[24] COVID-19 X-ray images, (n.d.). https://www.kaggle.com/bachrr/covid-chest-xray.

[25] Chest X-ray Images (Pneumonia), (n.d.). https://www.kaggle.com/paultimothymooney/chest-xray-pneumonia.

[26] L. Wang, P. Gong, G.S. Biging, Individual tree-crown delineation and treetop detection in high-spatial-resolution aerial imagery, Photogramm. Eng. Remote Sensing. 70 (2004) 351–357, http://dx.doi.org/10.14358/PERS.70.3.351.

[27] H. Huang, X. Li, C. Chen, Individual tree crown detection and delineation from very-high-resolution UAV images based on bias field and marker-controlled watershed segmentation algorithms, IEEE J. Sel. Top. Appl. Earth Obs. Remote Sens. 11 (2018) 2253–2262, http://dx.doi.org/10.1109/JSTARS.2018.2830410.

[28] A. Krizhevsky, I. Sutskever, G.E. Hinton, Imagenet classification with deep convolutional neural networks, in: Adv. Neural Inf. Process. Syst., 2012, pp. 1097–1105.

[29] K. Simonyan, A. Zisserman, Very deep convolutional networks for large-scale image recognition, 2014, ArXiv Prepr, arXiv:1409.1556.

[30] F. Demir, D.A. Abdullah, A. Sengur, A new deep CNN model for environmental sound classification, IEEE Access 8 (2020) 66529–66537, http://dx.doi.org/10.1109/ACCESS.2020.2984903.

[31] T. Li, C. Qing, X. Tian, Classification of heart sounds based on convolutional neural network, Commun. Comput. Inf. Sci. 819 (2018) 252–259, http://dx.doi.org/10.1007/978-981-10-8530-7_24.

[32] F. Demir, M. Turkoglu, M. Aslan, A. Sengur, A new pyramidal concatenated CNN approach for environmental sound classification, Appl. Acoust. 170 (2020) 107520, http://dx.doi.org/10.1016/j.apacoust.2020.107520.

[33] S. Ioffe, C. Szegedy, Batch normalization: Accelerating deep network training by reducing internal covariate shift, in: 32nd Int. Conf. Mach. Learn., Vol. 1, ICML 2015, 2015, pp. 448–456.

[34] F. Demir, A.M. Ismael, A. Sengur, Classification of lung sounds with CNN model using parallel pooling structure, IEEE Access 8 (2020) 105376–105383, http://dx.doi.org/10.1109/ACCESS.2020.3000111.

[35] S. Hochreiter, J. Schmidhuber, Long short-term memory, Neural Comput. 9 (1997) 1735–1780.

[36] Ü. Budak, Z. Cömert, Z.N. Rashid, A. Şengür, M. Çıbuk, Computer-aided diagnosis system combining FCN and Bi-LSTM model for efficient breast cancer detection from histopathological images, Appl. Soft Comput. J. 85 (2019) 105765, http://dx.doi.org/10.1016/j.asoc.2019.105765.

[37] N. Srivastava, G. Hinton, A. Krizhevsky, I. Sutskever, R. Salakhutdinov, Dropout: A simple way to prevent neural networks from overfitting, J. Mach. Learn. Res. 15 (2014) 1929–1958.

[38] V. Bajaj, S. Taran, E. Tanyildizi, A. Sengur, Robust approach based on convolutional neural networks for identification of focal EEG signals, IEEE Sensors Lett. 3 (2019) 1–4, http://dx.doi.org/10.1109/LSENS.2019.2909119.

[39] P.K. Sethy, S.K. Behera, P.K. Ratha, P. Biswas, Detection of coronavirus disease (COVID-19) based on deep features and support vector machine, Int. J. Math. Eng. Manag. Sci. 5 (2020) 643–651, http://dx.doi.org/10.33889/IJMEMS.2020.5.4.052.

[40] E.E.-D. Hemdan, M.A. Shouman, M.E. Karar, COVIDX-net: A framework of deep learning classifiers to diagnose COVID-19 in X-ray images, 2020, http://arxiv.org/abs/2003.11055, ArXiv Prepr, arXiv:2003.11055.

[41] Y. Song, S. Zheng, L. Li, X. Zhang, X. Zhang, Z. Huang, J. Chen, H. Zhao, Y. Jie, R. Wang, Y. Chong, J. Shen, Y. Zha, Y. Yang, Deep learning enables accurate diagnosis of novel coronavirus (COVID-19) with CT images, 2020, http://dx.doi.org/10.1101/2020.02.23.20026930, MedRxiv.

[42] S. Wang, B. Kang, J. Ma, X. Zeng, M. Xiao, J. Guo, M. Cai, J. Yang, Y. Li, X. Meng, B. Xu, A deep learning algorithm using CT images to screen for corona virus disease (COVID-19), 2020, http://dx.doi.org/10.1101/2020.02.14.20023028, MedRxiv.

[43] H. Panwar, P.K. Gupta, M.K. Siddiqui, R. Morales-Menendez, V. Singh, Application of deep learning for fast detection of COVID-19 in X-rays using nCOVnet, Chaos, Solitons and Fractals. 138 (2020) 109944, http://dx.doi.org/10.1016/j.chaos.2020.109944.

[44] M. Nour, Z. Cömert, K. Polat, A novel medical diagnosis model for COVID-19 infection detection based on deep features and Bayesian optimization, Appl. Soft Comput. J. 97 (2020) 106580, http://dx.doi.org/10.1016/j.asoc.2020.106580.